Published in final edited form as:

Cell. 2021 January 07; 184(1): 194–206.e14. doi:10.1016/j.cell.2020.11.038.

Structural basis of WLS/Evi-mediated Wnt transport and secretion

Rie Nygaard[1], **Jia Yu**[2], **Jonathan Kim**[1], **Daniel Ross**[1], **Giacomo Parisi**[1], **Oliver B Clarke**[1,3], **David M Virshup**[2,4,*], **Filippo Mancia**[1,5,*]

[1]Department of Physiology and Cellular Biophysics, Columbia University Irving Medical Center, New York, NY 10032, USA.

[2]Programme in Cancer and Stem Cell Biology, Duke-NUS Medical School, Singapore 169857.

[3]Department of Anesthesiology, Columbia University Irving Medical Center, New York, NY 10032, USA.

[4]Department of Pediatrics, Duke University School of Medicine, Durham, NC 27705, USA.

[5]Lead Contact

SUMMARY

Wnts are evolutionarily conserved ligands that signal at short range to regulate morphogenesis, cell fate and stem cell renewal. The first and essential steps in Wnt secretion are their O-palmitoleation and subsequent loading onto the dedicated transporter WLS/Evi. We report the 3.2 Å resolution cryo-EM structure of palmitoleated human WNT8A in complex with WLS accompanied by biochemical experiments to probe the physiological implications of the observed association. The WLS membrane domain has close structural homology to G protein-coupled receptors (GPCR). A Wnt hairpin inserts into a conserved hydrophobic cavity in the GPCR-like domain with the palmitoleate protruding between two helices into the bilayer. A conformational switch of highly conserved residues on a separate Wnt hairpin may contribute to its transfer to receiving cells. This work provides molecular-level insights into a central mechanism in animal body plan development and stem cell biology.

Graphical Abstract

*Correspondence to be addressed to: david.virshup@duke-nus.edu.sg. (D.M.V.) and fm123@cumc.columbia.edu (F.M.).

AUTHOR CONTRIBUTIONS

R.N. performed protein purification, cryo-EM data collection, structural refinement analysis and figure preparation. J.Y. carried out cloning, construct screening, mutagenesis, cell surface biotinylation, TOPFlash reporter assays, immunoprecipitation assays and figure preparation. J.K. expressed the protein and assisted with purification and preparation of the figures. D.R. contributed to protein purification and sample preparation for cryo-EM data collection. G.P. performed initial expression screening of constructs. O.B.C. provided critical insight in cryo-EM data processing, model building and refinement as well as preparation of the figures, and F.M. and D.M.V. co-led the project, designed experiments and wrote the manuscript with R.N., J.Y., D.R. and J.K.

DECLARATION OF INTEREST

The authors declare no competing interest.

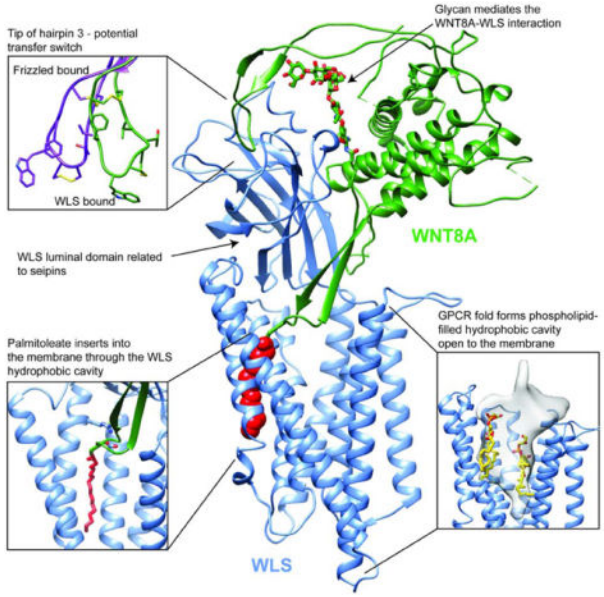

eTOC/In Brief:

The cryo-EM structure of palmitoleated human WNT8A bound to its transporter Wntless/WLS/EVI uncovers the mechanisms of Wnt secretion, revealing broad structural similarities to GPCRs and lipid-sensing pathways.

Keywords

Wnt signaling; palmitoleation; single-particle cryo-electron microscopy; membrane proteins; GPCR; Wntless; Frizzled; structural biology; membrane transport

INTRODUCTION

Wnts are a family of secreted, lipid-modified glycoproteins that regulate morphogenesis, stemness, and cell fate decisions. Upon reaching the membrane of a producing cell, Wnts travel locally through the extracellular space to nearby signal-receiving cells, where they interact with a diversity of cell-surface receptors, including a family of 10 human Frizzleds, as well as an increasing array of Wnt co-receptors such as LRP5/6 and the receptor tyrosine kinase ROR2 (Langton et al., 2016; Niehrs, 2012; Routledge and Scholpp, 2019). The Wnt-receptor interaction in turn triggers several different downstream signaling cascades including the stabilization of β-catenin, regulating changes in gene expression, and the activation of JNK, regulating changes in cell polarity. The multiple roles that Wnt family members play in body plan development and homeostasis across all animal species is highlighted by the diverse number of conserved paralogs present in different organisms: for example, the human and mouse genomes have 19 Wnt genes, while the sea anemone *Nematostella vectensis*, a cnidarian branch occurring prior to the advent of bilaterality, has at least 12 (Kusserow et al., 2005; Loh et al., 2016).

A central feature of Wnt biology is the requirement for the covalent attachment of a mono-unsaturated palmitoleate (PAM) to a serine residue that is conserved in essentially all Wnts (Takada et al., 2006) (Figure 1A). This unusual protein O-acylation renders Wnt proteins highly hydrophobic and dependent on carriers for both intra- and inter-cellular movement (Hannoush, 2015). Wnt palmitoleation is catalyzed in the endoplasmic reticulum by the membrane bound O-acyltransferase (MBOAT) porcupine (PORCN) (Kadowaki et al., 1996; van den Heuvel et al., 1993), in a reaction that requires mono-unsaturated palmitate in the form of palmitoleoyl-CoA (Rios-Esteves and Resh, 2013). Following acylation, Wnts become competent to bind in the ER to the conserved membrane transport protein variously known as Wntless (WLS), Evi, and GPR177 for transport across cellular compartments and secretion (Figure 1A) (Bartscherer et al., 2006; Bänziger et al., 2006; Coombs et al., 2010; Goodman et al., 2006; Herr and Basler, 2012; Najdi et al., 2012; Yu et al., 2014).

While multiple genes encode functional Wnts and their receptors, the secretory module of PORCN and WLS are each encoded by a single essential gene in all animal genomes. WLS is an integral membrane protein predicted to have eight transmembrane (TM) helices, with an extended luminal loop that has been shown to be essential for Wnt binding, and an ER recycling motif at the cytoplasmic C-terminus (Bartscherer et al., 2006; Bänziger et al., 2006; Coombs et al., 2010; Goodman et al., 2006; Yu et al., 2014). WLS has also been named GPR177 due to a proposed homology to G-protein coupled receptors (Gloriam et al., 2007). PORCN-catalyzed acylation of Wnts is absolutely required for them to bind to WLS in the ER (Coombs et al., 2012; Herr and Basler, 2012; Najdi et al., 2012). Mutations in the Wnt palmitoleation site, inhibition of PORCN, or downregulation of WLS expression all prevent Wnt ER exit and secretion (Moti et al., 2019; Takada et al., 2006; Yu et al., 2014). Loss of function mutations in *PORCN*, an X-linked gene, are lethal in males (Grzeschik et al., 2007; Wang et al., 2007), while drugs that inhibit PORCN are effective treatment for Wnt-addicted cancers in preclinical models and are currently in ongoing clinical trials (Zhong and Virshup, 2020). Similarly, whole body knockout (KO) of *Wls* is lethal in mice (Fu et al., 2009) and tissue-specific KO models display various Wnt-related phenotypes (Carpenter et al., 2010; Zhong et al., 2012). Thus, the PORCN-WLS acylation-secretion module is required and essential for all Wnt function.

Wnts are short range signaling molecules, and the role of WLS in this process remains unclear. In the journey from the ER to the plasma membrane, the Wnt-WLS complex traverses the Golgi where additional Wnt glycosylation occurs, to reach the plasma membrane. Wnt glycosylation may determine differential targeting of the Wnt-WLS complex to different exit sites on polarized cells (Yamamoto et al., 2013). The covalently attached O-palmitoleate restricts how Wnts travel after they reach the cell membrane, where they must be transported by one of several forms of facilitated diffusion to reach their receptors on neighboring cells. The Wnt-WLS complex may transfer Wnts to cell surface proteoglycans, to soluble transport proteins, to cytonemes, or to exosomes (McGough et al., 2020; Routledge and Scholpp, 2019). Ultimately, in a step which is again dependent on the presence of the O-palmitoleate, Wnts are delivered to Frizzled (FZD) and its associated co-receptors on the surface of the receiving cells to initiate downstream signaling (Niehrs, 2012; Yu et al., 2014). WLS can then recycle from the plasma membrane back to the ER for

additional cycles of Wnt transport (Belenkaya et al., 2008; Franch-Marro et al., 2008; Yu et al., 2014).

Structural studies of Wnt pathway proteins have provided important insights into how signal transduction occurs. Given the fact that acylated Wnts are highly insoluble, the structure of palmitoleated Wnt was first determined only after it was purified in a complex bound to its receptor, the cysteine-rich domain (CRD) of FZD (Hirai et al., 2019; Janda et al., 2012). There, the PAM lies in a hydrophobic groove in the CRD in the extracellular space, where it may provide a signal for receptor dimerization (Nile et al., 2017). The structures of xWnt8 and WNT3 in complex with the FZD CRD, coupled with evolutionary analysis, revealed that Wnts are composed of two major domains (Bazan et al., 2012; Hirai et al., 2019; Janda et al., 2012). An amino-terminal core domain (NTD) distantly related to saposins contains multiple helices in an anti-parallel bundle from which extends hairpin 1 and the PAM-containing hairpin 2. The carboxyl-terminal domain (CTD) comprises hairpin 3 and is structurally related to cysteine-knot growth factors. Wnt hairpins 1 and 2 contact Frizzled CRD site 1, and hairpin 3 contacts CRD site 2. Isolated Wnt NTD or CTD domain constructs can interfere with Wnt signaling, suggesting they retain some ability to compete with intact Wnts for binding to the CRD (Hoppler et al., 1996; Janda et al., 2012; Kumar et al., 2014). Indeed, isolated hairpin 3 of the CTD can interact with the FZD CRD and function as a mini-Wnt, and mutation of highly conserved residues on its tip impairs signaling ability (Janda et al., 2012; Kumar et al., 2014).

How a newly palmitoleated Wnt is transferred from PORCN to WLS, how the three components – Wnt, the O-palmitoleate, and WLS – assemble in an energetically favorable and transport-efficient complex, and how Wnt is transferred from WLS to various transporters and to FZD on the neighboring cell remains poorly understood.

RESULTS

Expression and purification of the human WNT8A-WLS complex

To gain structural insights into the association of palmitoleated Wnts with WLS, multiple Wnts were screened for expression and complex formation with WLS by transient transfection of mammalian cells. We chose to work on human WNT8A and human WLS based on activity, expression levels and detergent stability of the complex (Figure S1A, S1B and S1C). We confirmed that formation of the palmitoleation-dependent WNT8A-WLS complex is required to transport both components to the cell surface (Figure 1B) (Coombs et al., 2010; Herr and Basler, 2012). WNT8A and WLS were co-expressed in HEK293S GnTI^{-} cells (Reeves et al., 2002) by co-transduction of two separate baculoviruses prepared with the BacMam system (Goehring et al., 2014). The WNT8A-WLS complex was purified in detergent and reconstituted in lipid-filled nanodiscs using a different affinity tag on each protein to ensure a homogenous preparation (Figure S1D, S1E and S1F). The structure of the 101 kDa WNT8A-WLS complex was determined to a nominal resolution of 3.2 Å by single-particle cryo-electron microscopy (cryo-EM) (Figure 1C, Figure S2 and Table S1). A model was built comprising residues 4–496 from the 541 amino acid WLS, and residues 30–337 of the 351 amino acid WNT8A (Figure 1D, 1E and Figure S3), lacking the C-terminal

tail of WLS (residues 497–541) and three loop segments in WNT8A – 115–125, 223–240, and 279–287 – which were disordered.

WLS has eight transmembrane helices and a globular disulfide-stabilized luminal domain

The structure of WNT8A-bound human WLS reveals two distinct components: an integral membrane domain composed of eight TM helices with both N- and C-termini on the cytosolic side, and a globular luminal domain (WLS-LD) between TM1 and TM2, known to be required for Wnt binding (Figure 1D, 1E) (Coombs et al., 2010). The WLS-LD, largely encoded by exons 2–4 (Figure S4), forms a compact structure of eight antiparallel β-sheets, resembling a β-sandwich (Figure 1D and 1E). There are four cysteines in the WLS-LD that are conserved in essentially all eukaryotic WLS (Figure S4). They appear to form two disulfide bonds, linking β-strands 5 and 6 and stabilizing the loop region between β–strand 1 and 2 (Figure S5A). Mutation of any of these cysteines markedly impairs WLS activity (Figure S5B). WLS has a conserved clathrin-mediated endocytosis motif YXXΦ at residue Tyr425, where Φ is a bulky hydrophobic residue (Gasnereau et al., 2011; Yu et al., 2014). This motif is located on an intracellular loop between TM helices 6 and 7, conceivably well positioned to engage with the endocytosis machinery (Figure S5A).

A structural homology search reveals that the WLS-LD resembles seipin (RMSD of ~1.3 Å), an ancient ER protein involved in lipid droplet formation (Figure S5C) (Sui et al., 2018; Yan et al., 2018). Moreover, seipin appears to also be topologically similar, with two TM domain anchors flanking eight antiparallel β-sheets in the ER lumen, closely resembling the TM1-WLS-LD -TM2 arrangement observed in WLS. Consistent with the proposed origins of Wnts from lipid-sensing pathways, the WLS seipin homology domain makes contacts with the helical core of Wnt that has structural homology to saposins, another ancient protein implicated in lipid metabolism (Bazan et al., 2012).

WNT8A-specific glycosylation at the interface with WLS

Different Wnts are N-glycosylated at several distinct sites and this glycosylation may play a role in Wnt-WLS sorting during secretion (Yamamoto et al., 2013). Our structure shows two sites on WNT8A, Asn103 and Asn262, that contain N-linked glycans (Figure 2A and 2B). These residues are similarly glycosylated in the xWnt8 structure (Janda et al., 2012). The Asn103 site is unique to the WNT8 family, while Asn262 is also found in WNT5A/B (Asn312 of human WNT5A) (Figure S7). The glycan attached to Asn262 is near the proposed LRP5/6 binding site (Hirai et al., 2019) and could influence co-receptor interactions. The glycan attached to WNT8A at position Asn103 is in close proximity to an extensive hydrophilic surface of WLS, seemingly mediating the interaction between the two proteins in this region (Figure 2C). Mutation of Asn103 impaired both the production and the signaling activity of WNT8A, suggesting an important functional role for this glycan (Figure 2D and 2E).

Wnt hairpins are central to the interaction with WLS

Similar to Wnts in complex with the FZD CRD (Hirai et al., 2019; Janda et al., 2012), the structure of WNT8A when in complex with WLS has a highly conserved core of five helices from which the three hairpin loops extend, and two of these loops – hairpins 2 and 3 –

assemble as β–strands forming β-sheets (Figures 1E and S6). The interaction between WNT8A and WLS is extensive, consisting of 2403 $Å^2$ of buried surface (Figures 2A, 2B and S6), likely contributing to the tight binding between the two proteins (Coombs et al., 2010; Janda et al., 2012).

Wnt hairpin 1, which in the Wnt-CRD structure interacts directly with hairpin 2, here instead is separated from hairpin 2 by the first β–sheet of the WLS-LD (Figure 2A and 2B). Hairpin 1 extends two conserved tryptophan residues Trp127 and Trp129 to foster a number of contacts with highly conserved WLS residues including Ser104, Phe107, Asn227, and Gly229 on the top of WLS TM helices 1 and 2 (Figure 3A).

Hairpin 2, stabilized by two disulfide bonds, carries the PAM at its tip bound to the absolutely conserved Ser186. This hairpin inserts deep into the WLS TM domain and makes multiple contacts within a central hydrophobic cavity also lined by conserved residues (Figure 3B). The PAM in turn threads through a narrow hydrophobic tunnel between TM helices 4 and 5 facilitated by WLS Gly305 (Figure 3C and 3D). The WNT8A Ser186-palmitoleate ester bond is coordinated primarily by an ionic interaction between WLS Asp301 and WLS Arg357 (Figure 3D). The density map does not clearly define the position of the distal carbons of the PAM, consistent with it being flexible within the lipid bilayer (Figure S3). This suggests that WLS, similar to both the FZD CRD and the recently observed palmitate binding site of the *Drosophila* glypican Dlp, may not be highly sensitive to acyl chain length (McGough et al., 2020; Nile et al., 2017). This observation is in contrast to the high specificity reported for PORCN and the Wnt deacylase NOTUM for 16:1 acyl groups (Kakugawa et al., 2015; Lee et al., 2019; Rios-Esteves and Resh, 2013; Tuladhar et al., 2019).

As a biochemical test of the model, we replaced WNT8A hairpin 1 contact points, including WLS residues Ser104, Phe107, and Asn227 with alanine, or in the case of Gly229, with glutamine. These changes significantly impaired the ability of Wnt to signal to β-catenin in a TOPFlash reporter assay (Figure 3E) (Swiatek et al., 2006). We next mutated WLS residues with a role in hairpin 2 binding. Loss of the WLS Asp301-Arg375 interaction that coordinates the serine-PAM bond completely abrogated Wnt signaling. Replacement of Gly305 in TM4 that interacts with PAM, with a bulky tryptophan residue (G305W) markedly decreased signaling as well (Figure 3E).

To better understand the nature of the impaired signaling activity, we assessed the ability of various WLS mutants to bind to and promote secretion of WNT8A (Figures 3F, 3G). Virtually all mutants of WLS that affected its interaction with Wnt hairpins 1 and 2 decreased Wnt secretion into the medium (Figure 3F). Mutants S104A and G229Q were expressed comparably to WT but had decreased Wnt binding and secretion. Several mutants (e.g. N227A) had both decreased expression and decreased secretion. The decreased ability of these mutants to bind to WNT8A was also found in a co-immunoprecipitation assay (Figure 3G). These data indicate that there are multiple important interactions of WLS with Wnt hairpins 1 and 2 essential for retrieving newly synthesized, palmitoleated Wnts from the ER.

A conformational switch in Wnt hairpin 3

In the WNT8A-WLS structure, hairpin 3 forms an arch from the helical core to the upper extremity of the WLS-LD (Figure 1E and 2A) where it inserts Trp318 of the sequence Trp-Cys-Cys deep into a conserved, hydrophobic pocket (Figure 2B, 4A and 4C). Consistent with the conserved nature of the tip of Wnt hairpin 3 (Figure 4B and S7), this binding pocket on WLS can likely accommodate a variety of Wnts. One notable change in Wnt hairpin 3 in moving from its interaction with WLS to the FZD CRD is the orientation of Phe316 and Trp318. The sidechains of these residues shift markedly between the two structures (Figure 4C), suggesting they may function as a molecular switch when Wnt changes binding partners.

Wnt hairpin 3, while essential for interaction with the FZD CRD, is apparently not required for Wnt secretion. Mutation of a number of conserved residues within this hairpin abrogates Wnt signaling activity without impairing Wnt secretion (Kumar et al., 2014; Macdonald et al., 2014; Speer et al., 2019). Similarly, Wnts lacking this hairpin can also be secreted (Hoppler et al., 1996; Kumar et al., 2014; Wu and Nusse, 2002). We confirmed that WNT8A with mutation of either Trp318, Cys319 or Cys320 to alanine were able to be secreted but were unable to signal (Figure 4D and 4E) (Macdonald et al., 2014). This suggests that the conserved WCC motif that interacts with the WLS-LD is required, not because it binds to WLS, but because it allows Wnt hairpin 3 to transfer to and interact with the FZD CRD.

In the xWnt8-FZD CRD and the WNT3A-CRD structures, Wnt hairpin 3 is stabilized by three highly conserved disulfide bonds, including an unusual vicinal disulfide bond between Cys319 and Cys320 in the WCC motif (Figure 4A, Figure 4C) (Hirai et al., 2019; Janda et al., 2012). The densities at Cys319 and Cys320 do not allow a firm conclusion as to whether they are oxidized or reduced (Figures 4A, 4C and S3); in the deposited model (PDB 7KC4) we present the oxidized form. The mutational studies noted above suggest formation of the disulfide bond is not essential for palmitoleation and WLS interaction, but is necessary for WNT3A to bind to the FZD CRD (Macdonald et al., 2014). These data support the importance of Wnt hairpin 3 for association with the FZD CRD rather than for interaction with WLS.

Flexibility in the Wnt hairpins allows binding to WLS and the FZD CRD

A comparison of the two structures, WNT8A in complex with WLS, and xWnt8 in complex with FZD, shows essentially no differences in the α-helix core of the Wnts, but substantial movements in the hairpin loops (Figure 5). WNT8A hairpins 1 and 2 are moved apart by the WLS-LD (aa 39–47). In the Wnt-CRD structure these two hairpins are tightly associated and form a partial β-sheet (Figure 5B). When bound to WLS, WNT8A hairpin 1 is displaced laterally by 22.6 Å, hairpin 3 shifts inwards by 17.2 Å to contact the WLS hydrophobic pocket, and hairpin 2 with the attached PAM is moved by 15.4 Å as measured from Ser186 in WNT8A, to insert the PAM into the TM domain of WLS (Figure 5C). These movements indicate substantial flexibility in the Wnt hairpins that may also contribute to their versatility in being able to bind to other Wnt-interacting proteins such as PORCN, RYK, ROR1, GPC4 and PTK7 (Niehrs, 2012).

The hydrophobic nature of a WLS central cavity within the TM domain

One of the most surprising findings in the structure of WLS is a large cavity buried deep within the WLS TM domain. This space is open to the luminal side at the top, and to the lipid bilayer via a gap between TM helices 6 and 7, suggesting a potential avenue for palmitoleated Wnt hairpin 2 to enter and exit (Figure 6A). The density map also reveals the presence of additional species inside this cavity, which we tentatively assigned to two POPG (1-palmitoyl-2-oleoyl-3-*sn*-phosphatidyl glycerol) molecules, the lipids that were used for nanodisc reconstitution (Figure 6B). These ordered POPG molecules contact the conserved inner lining of the WLS binding pocket (Figure 6C). We note that POPS (1-palmitoyl-2-oleoyl-*sn*-glycero-3-phospho-L-serine) was required for solubilization of active PORCN (Lee et al., 2019), suggesting that common membrane components such as glycerol-phospholipids might play a role in stabilizing the interactions between protein and PAM, or contributing to an energetically favorable environment as the PAM enters or exits the WLS central cavity.

WLS has homology to G-protein coupled receptors

Despite its original name of GPR177 and the evolutionary conservation of the multiple TM domains (Figure S4) (Gloriam et al., 2007), the structural homology of WLS to the GPCR family has remained unclear. A search of the Protein Database with the WLS TM domain using the DALI server (Holm, 2020) identified GPCRs including Smoothened (PDB ID 6D35 and 6O3C) (Deshpande et al., 2019; Huang et al., 2018), Frizzled 4 (PDB ID 6BD4) (Yang et al., 2018) and the glucagon receptor (PDB ID 5YQZ) (Zhang et al., 2018a), as proteins with the highest structural similarity. We aligned WLS TM helices 2–8 with both the glucagon receptor and Frizzled 4 (RMSD for the Cα backbone 1.0 and 1.1 Å, respectively), and confirmed they indeed have very similar arrangements within the membrane (Figure 6D and 6E). WLS lacks the classical cytoplasmic helix 8 found in most GPCRs that is parallel to the membrane plane. The WLS central hydrophobic cavity where PAM and WNT8A hairpin 2 interact corresponds to the canonical GPCR ligand-binding site (Figure 6F). While phospholipids are not generally observed in GPCR binding sites, ligands for GPCRs can be hydrophobic (Audet and Stevens, 2019), and the structure of the $GABA_B$ receptor shows evidence of a bound ordered phosphatidylethanolamine (Papasergi-Scott et al., 2020; Park et al., 2020). In other GPCRs, small drug-like molecules can insert into smaller versions of this cavity to regulate function (Zhang et al., 2018b). WLS similarly may be able to accommodate small molecules in this domain, making it a potential target for drugs that would inhibit the secretion of all Wnts.

DISCUSSION

WLS is the link between Wnt synthesis and Wnt receptor engagement and is required to transport the large number (19 in human) of Wnts from their site of synthesis in the endoplasmic reticulum onwards towards the variety of Wnt transporters and receptors on nearby cells. Using single-particle cryo-EM, we determined the structure of human palmitoleated WNT8A in complex with WLS. The structure reveals that WLS has an ancient – and potentially druggable – GPCR fold within its TM domain, and a luminal domain apparently related to an ancient lipid-binding fold. The Wnt hairpin 2 bearing the O-linked

PAM extends deep into a conserved hydrophobic cavity in the GPCR-like domain (Figure 2B), in a region that has been targeted by small molecules in other GPCRs (Figure 6F). There are extensive contacts between Wnt and WLS in the LD as well. The combination of these hydrophobic PAM-WLS-bilayer and charged Wnt hairpin 2-WLS interactions likely explain the previously observed tight binding between Wnts and WLS (Coombs et al., 2010). However, the contacts of Wnt hairpin 3 appear to be dispensable for binding to WLS, while essential for interaction with the FZD CRD.

The structure of WNT8A-WLS suggests a model for how Wnts might be transferred in the ER from PORCN to WLS. The WLS central cavity has a large opening to the lipid bilayer between TM helices 6 and 7 (Figure 6A). This opening may be ideally suited to accommodate the lateral transfer in *cis*, i.e. within the same membrane, of palmitoleated Wnt from PORCN (Figure 7). Conserved residues on the surface of the TM domain of WLS near this opening (Figures 2B, 6A and S6A) may serve as contact points for WLS to bind to PORCN to facilitate the transfer. This direct transfer model is consistent with previous findings that PORCN expression causes clustering of endogenous WLS in the ER (Yu et al., 2014). More speculatively, the loading of palmitoleated Wnt onto WLS could also trigger a conformational change of the WLS TM domains that may in turn serve as a signal for the Wnt-WLS complex to exit the ER and travel to the plasma membrane.

The structure resolves the persistent question of how WLS handles the PAM moiety bound to Wnt. When Wnt covalent O-acylation was first identified, speculation centered on a membrane-tethering or lipoprotein-binding role for the fatty acid, similar to the role the far more common S-palmitoylation plays in diverse proteins (Panáková et al., 2005; Smotrys and Linder, 2004; Takada et al., 2006; Willert et al., 2003). A number of PAM-binding proteins including various MBOAT proteins and stearoyl CoA desaturase also accommodate the acyl group in the plasma membrane (Sui et al., 2020; Wang et al., 2015). Conversely, the structure of xWnt8 in complex with the FZD CRD demonstrated that the PAM could instead be accommodated in a hydrophobic groove in the extracellular space (Nile et al., 2017). More recently, the structures of Notum, a Wnt deacylase, and Dally-like protein (Dlp), a GPI-anchored glypican that facilitates Wnt diffusion on cell surfaces, also demonstrated binding of PAM to domains in the extracellular space (Kakugawa et al., 2015; McGough et al., 2020). We had previously speculated that the WLS luminal domain might harbor a PAM-binding site (Coombs et al., 2010). However, the WNT8A-WLS structure demonstrates that the PAM remains firmly anchored in the central cavity and adjacent lipid bilayer of the GPCR-like TM domain.

How Wnts are released at the plasma membrane remains controversial. The WNT8A-WLS structure provides some insight into mechanisms of Wnt secretion. The commonly accepted *trans*-transfer model proposes that Wnts are released from WLS at the surface of sending cells and undergo facilitated diffusion towards Wnt receiving cells via interaction with glypicans and/or lipid binding proteins (Langton et al., 2016; McGough et al., 2020; Routledge and Scholpp, 2019; Stanganello and Scholpp, 2016) (Figure 7). An alternative mechanism that may be operative in some settings is the transfer of Wnt from WLS to FZD receptors in *cis*, for example, after vesicular transport of a Wnt-WLS complex to a receiving cell. This model is consistent with data that (i) Wnts can signal in an autocrine manner, (ii)

Wnt and WLS can transfer together across synapses on lipid vesicles such as exosomes, and (iii) WLS and Wnt are transferred together to the receiving cell membrane in the *Drosophila* brain (Gross et al., 2012; Koles et al., 2012; Korkut et al., 2009). Constraining both of these models is the fact that the PAM of Wnt is buried deep in the lipid bilayer when bound to WLS, contributing to a seemingly tight interaction. Our prior study indicated that vesicular acidification was required for Wnt transfer from WLS (Coombs et al., 2010). Our structure shows a histidine in Wnt hairpin 2 (His183; Figure 3D) whose protonation might affect the Wnt-WLS interaction. However, mutation of this histidine was previously shown to block palmitoleation and hence WLS binding (Lee et al., 2019), hindering further analysis of its potential role in Wnt release. In either case, close interactions must be required to facilitate the extraction of PAM from WLS and the lipid bilayer into, e.g., the FZD juxtamembrane CRD hydrophobic groove, or the glypican PAM binding site. In the case of FZD and perhaps also glypicans, this may require or be triggered by the transfer of Wnt hairpin 3 from WLS to the respective CRD.

An intriguing change that occurs when Wnt moves from WLS to the FZD CRD is the conformational change of the highly conserved hairpin 3 (Figure 4B) that is proposed to be the major determinant of FZD binding affinity (Janda et al., 2012). In particular, the sidechains of Phe316 and Trp318 undergo a marked pivot. In addition, when bound to the FZD CRD, Wnt hairpin 3 has a vicinal disulfide bond at its tip. Vicinal disulfide bonds are rare, as they form a constrained eight-atom ring (Carugo et al., 2003; Hunter et al., 2002; Luken et al., 2010). We confirmed the previous observation that mutation of either or both cysteines had no effect on Wnt secretion but abrogated Wnt signaling activity (Figures 4D and 4E) (Macdonald et al., 2014). Consistent with these mutational data, our structure suggests that disulfide bond formation is not required for hairpin 3 to insert Trp318 of the WCC motif into its binding pocket on WLS. The side chains of Phe316 and Trp318 are clearly defined in the experimental density map and these residues adopt the same conformation regardless of how we model the vicinal cysteines, for which the density is ambiguous (Figure 4C and Figure S3). We speculate that formation of the vicinal disulfide bond could be coupled to the dissociation of Wnt from WLS in the oxidizing extracellular milieu, thus licensing Wnt to bind to the FZD CRD, a hypothesis that will require further study.

To conclude, the structure of Wnt in complex with its obligate carrier protein WLS provides several insights into Wnt signaling. The multi-phyla conservation of the contact points between these two proteins suggests that WLS-mediated transport of lipid-modified Wnt is an ancient and essential step in the pathway and provides an explanation for why WLS can bind to all Wnts. The structure appears to settle the longstanding question of whether WLS is closely related to GPCRs, showing WLS indeed has a GPCR-related fold in its TM domain. Unique to WLS is a luminal domain that makes extensive contacts with the Wnt hairpins, and an extensive central hydrophobic cavity within the GPCR-like TM domain, which is open to the membrane and harbors both the PAM and ordered glycerol phospholipids, likely important for stabilization of the PAM. The insertion of the PAM into the lipid bilayer provides constraints for models of how Wnts are transferred from PORCN to WLS, and then onto their receptors on nearby cells. Wnt hairpin 3 may serve as a conformational switch with implications for both the localization and unidirectionality of the

transfer of Wnt between WLS and the FZD CRD. The structure of the WNT8A-WLS complex establishes a framework to understand at a molecular level how this key developmental and homeostatic pathway establishes short range signaling.

STAR METHODS

RESOURCE AVAILABILITY

Lead Contact—Further information and requests for resources and reagents should be directed to and will be fulfilled by the Lead Contact, Filippo Mancia (fm123@cumc.columbia.edu).

Material Availability—All unique/stable reagents generated in this study are available from the Lead Contact with a completed Materials Transfer Agreement. Plasmids generated in this study are available upon request.

Data and Code Availability—The datasets generated during this study are available at PDB: 7KC4, EMD-22806 and EMPIAR-872.

EXPERIMENTAL MODEL AND SUBJECT DETAILS

DH10Bac *E. coli* competent cells were used to generate recombinant baculovirus for heterologous protein expression. STF cells and RKO WLS knockout cells were previously reported (Coombs et al., 2010; Moti et al., 2019; Xu et al., 2004). HEK293 and RKO cells were cultured in DMEM medium supplemented with 10% fetal bovine serum (FBS) (HyClone), 1% penicillin and streptomycin (Invitrogen) and 1% sodium pyruvate (Lonza) at 37 °C and 5% CO_2.

METHOD DETAILS

Plasmids and reagents—To identify suitable candidates for structural studies, human WNT3A, 7A and 8A with a C-terminal StrepII-tag and human WLS isoform 1 with C-terminal GFP and 10×-histidine tags were cloned into pcDNA3.1 vector for transient transfection in mammalian cells. To scale up protein expression, Human WNT8A with a StrepII-tag, and human WLS isoform 1 with C-terminal 10× histidine and FLAG tag (Fig. S1D) were both cloned into the pEG BacMam vector (Goehring et al., 2014) for baculovirus transduction of mammalian cells. The final constructs were verified by Sanger sequencing. The PORCN inhibitor ETC-159 was formulated in DMSO and used at a final concentration of 100 nM as previously described (Madan et al., 2016).

Wnt/β-catenin reporter assay—One day before transfection, RKO WLS null cells were seeded into 24-well plates. Cells were transfected using Lipofectamine 2000 (Thermo Fisher) mixed with DNA in a ratio of 3:1 using the manufacturer's protocol. For each well 100 ng STF reporter, 50 ng mCherry, 50 ng PGK-mWNT3A and indicated amount of WLS plasmid mix was used. After 48 hours of transfection, cells were lysed with 100 μl of Reporter Lysis Buffer (Promega) supplemented with protease inhibitor cocktail (Roche) for 20 minutes at 4 °C with shaking. The cell lysates were transferred to a 96-well black plate and then an equal volume of luciferase assay reagent (Promega) was added. Luciferase

activity was measured on a Tecan Infinite 2000 plate reader. mCherry values were used for normalization.

Transient protein expression and fluorescent size exclusion chromatography—10 ml of HEK293 Freestyle suspension cells at 2 × 10^6 cells/ml were co-transfected by mixing 7.5 μg of WLS plasmid and 7.5 μg of respectively the 3 different isoforms of WNT3A, WNT7A and WNT8A diluted into 500 μl opti-MEM (Thermo Fisher Scientific) with 60 μg of polyethylenimine (PEI) Max MW 40,000 (Polysciences) diluted into 500 μl opti-MEM. Cells were incubated for 72 hours at 37 °C in 7% CO^2 and 70% humidity before harvesting at 800×*g* for 20 minutes. Each pellet was resuspended and solubilized in 1 ml of a buffer containing 20 mM HEPES pH 7.5, 200 mM NaCl, 0.5 mM phenylmethylsulfonyl fluoride (PMSF), cOmplete™ EDTA-free protease inhibitor cocktail (Roche), 10 μg/ml DNase I (Roche), 8 μg/ml RNase (Sigma-Aldrich) and 1% n-dodecyl-β-D-maltopyranoside (DDM) with 0.1% cholesteryl hemisuccinate (CHS) at 4 °C for 2 hours with gentle agitation. Insoluble material was removed by ultracentrifugation for 45 minutes at 4 °C in a single angle rotor at 100,000×*g* in a TLA-120.2 rotor (Beckman Coulter). The supernatants were applied to 50 μl streptavidin resin (IBA) and incubated for 3 hours at 4 °C with gentle agitation in order to bind the strep-tagged Wnts. The resin was washed with 10 column volumes of a buffer containing 50 mM TRIS pH 8, 150mM NaCl, and 0.1% of DDM with 0.1% CHS. Elution was performed with 3 column volumes of the same buffer containing 50 mM biotin. The supernatant of each sample was subjected to fluorescence-coupled size exclusion chromatography (FSEC) analysis in a buffer containing 20 mM HEPES pH 7.5, 200 mM NaCl, 0.03% DDM with 0.003% CHS to evaluate both expression and stability of GFP-tagged WLS complex formation with Wnts.

WNT8A/WLS protein expression, purification and reconstitution into nanodiscs—Recombinant P1 baculovirus DNA was transfected into Sf9 cells (Expression System) in the presence of PEI and cultured in ESF 921 protein-free insect cell culture medium (Expression Systems). For protein expression, 75 ml WNT8A P4 virus and 25 ml WLS P4 virus were used to co-infect 1-liter cultures of HEK293S GnTI$^-$ cells (Reeves et al., 2002) (Invitrogen) at 3 × 10^6 cells/ml in Freestyle 293 medium (GIBCO) supplemented with 2% FBS (GIBCO). GnTI$^-$ cells lack N-acetylglucosaminyltransferase I (GnTI) activity, and so express more homogenously glycosylated proteins (Reeves et al., 2002). Cells were incubated for 16 hours at 37 °C in 8% CO_2 and 70% humidity before addition of 5 mM sodium butyrate (Sigma-Aldrich) to increase protein expression. Cells were further incubated at 37 °C for 48 hours before harvesting. Cell pellets were homogenized using low-salt buffer (100 mM Tris pH 8, 10 mM KCl, 10 mM $MgCl_2$, 0.5 mM PMSF, cOmplete EDTA™-free protease inhibitor cocktail, 10 μg/ml DNaseI and 8 μg/ml RNase) in a Dounce homogenizer before ultracentrifugation at 134,000×g in a type 45 Ti rotor (Beckman Coulter). Membrane fractions were further homogenized and washed using high-salt buffer (100 mM Tris pH 8, 500 mM NaCl, 10 mM KCl, 10 mM $MgCl_2$, 0.5 mM PMSF, cOmplete EDTA™-free protease inhibitor cocktail, 10 μg/ml DNase I and 8 μg/ml RNase) followed by ultracentrifugation. The washed membrane fractions were resuspended in storage buffer (100 mM Tris pH 8, 150 mM NaCl, 0.5 mM PMSF, cOmplete EDTA™-free protease inhibitor cocktail, 10 μg/ml DNaseI and 8 μg/ml RNase) using a Dounce homogenizer and

stored at −80 °C until use. Thawed membrane fractions were solubilized using DDM with CHS at a 10:1 (w/w) ratio to make a final concentration of 1% (w/v) detergent and incubated at 4 °C for 2 hours with gentle agitation. Insoluble material was pelleted by ultracentrifugation at 134,000×*g* in a type 45 Ti rotor (Beckman Coulter) for 30 minutes at 4 °C. The supernatant was added to a 50 ml conical tube containing pre-equilibrated Ni^{2+}-NTA resin (Qiagen) in 20 mM imidazole and incubated at 4 °C overnight with gentle agitation. Resin was washed with 10 column volumes of wash buffer (100 mM Tris pH 8, 200 mM NaCl, 20 mM imidazole, 0.05% DDM and 0.005% CHS), and eluted with 3 column volumes of elution buffer (100 mM Tris pH 8, 200 mM NaCl, 200 mM imidazole, 0.05% DDM and 0.005% CHS). Eluted protein was de-salted using a PD10 de-salting column (Millipore Sigma) using a buffer consisting of 100 mM Tris pH 8, 200 mM NaCl, 0.05% DDM and 0.005% CHS. De-salted eluent was concentrated to 0.56 mg/ml using a 50 kDa filter (Amicon). The eluent was incubated with a 1:5:300 molar ratio of protein:membrane-scaffold protein 1E3D1 (MSP1E3D1):1-palmitoyl-2-oleoyl-sn-glycero-3-phospho-(1′-rac-glycerol) (POPG) at 4 °C for 2 hours with gentle agitation to incorporate protein into nanodiscs. For reconstitution, detergent was removed from the mixture by incubating with Bio-beads (Bio-Rad) at 4 °C overnight with rotation. After separation of reconstituted nanodiscs from Bio-beads, the mixture was bound to pre-equilibrated streptavidin resin (IBA) through overnight rotation at 4 °C to remove empty nanodiscs and further purify the WNT8A/WLS complex. The streptavidin resin was washed with 10 column volumes of wash buffer (100 mM Tris pH 8, 150 mM NaCl) and nanodisc-protein complex was eluted using 3 column volumes of elution buffer (100 mM Tris pH 8, 150 mM NaCl, 50 mM biotin). Eluent was de-salted using a PD10 de-salting column (Millipore Sigma) with an elution buffer (100 mM Tris pH 8, 150 mM NaCl).

Single-particle cryo-EM vitrification and data acquisition—The purified protein complex was concentrated to 1.0 mg/ml using a 50 kDa filter concentrator (Amicon). The sample was frozen using a Vitrobot (Thermo Fisher) by adding 3 ul of the purified protein complex to previously plasma cleaned (Gatan Solarus) 0.6/1-μm holey gold grid (Quantifoil UltrAuFoil). After a 30 seconds incubation at 4 °C and >95% humidity, the grids were blotted using 595 filter paper (Ted Pella, Inc) for 7.5 seconds and immediately plunged into liquid ethane for vitrification. Images were recorded using a Titan Krios electron microscope (FEI), at the Columbia University Cryo-Electron Microscopy center, equipped with an energy filter and a K3 direct electron detection filter camera (Gatan K3-BioQuantum) using a 0.83Å pixel size.

An energy filter slit width of 20 eV was used during the collection and was aligned automatically every hour using the Leginon software package (Suloway et al., 2005). Data collection was performed using a dose of around 58 e^{-} $Å^{-2}$ across 50 frames (50 ms per frame) at a dose rate of approximately 16 e^{-} per pixel per s, using a set nominal defocus range of −1 μm to −2 μm. A 100-μm objective aperture was used. We collected a total of 12,747 micrographs over a 2.5 day session. The ice thickness, measured in Leginon using a coefficient calculated based on the zero loss peak, was determined to be 26.7 ± 16.1 nm (mean ± s.d).

Data processing—Movie frames were aligned using Patch Motion Correction implemented in cryoSPARC v.2.15 (Punjani et al., 2017) using a B-factor during alignment of 500. Contrast transfer function (CTF) estimations were done using Patch CTF implemented in cryoSPARC v.2.15 (Punjani et al., 2017). The micrographs were sorted based on CTF fit resolution, ice thickness and astigmatism and 3,642 micrographs were removed, resulting in 9,105 micrographs. Template picker in cryoSPARC v.2.15 was used to pick 4,415,933 particles, using templates from previous rounds of data processing derived from manually picked particles and filtered to 20 Å. The particles were extracted using a 320-pixel size box and binned four times and were then classified using 2D classification in cryoSPARC v.2.15 using a batchsize per class of 400 and "Force Max over poses/shifts" turned off with 40 online-EM iterations. 2D classes corresponding to intact particles with evident secondary structure were selected, resulting in a set of 188,472 particles after multiple rounds of 2D classification. *Ab initio* reconstruction was performed in cryoSPARC v.2.15 using three classes and a class similarity parameter of 0.1. Only one of the three classes, comprising 80,268 particles, displayed features consistent with a nanodisc-embedded membrane protein. These particles were re-extracted using a 320-pixel box size without binning. Heterogenous refinement using four starting models was done sequentially five times using the three previously obtained ab initio models plus a fourth class using an ab initio model generated from previously discarded particles. Non-uniform refinement of the final particle stack of 27,288 particles in cryoSPARC yielded a reconstruction with a resolution of 3.61 Å (FSC=0.143). The particles were re-extracted using a 450-pixel size box and subjected to a new non-uniform refinement, followed by a local non-uniform refinement using a mask around WLS and WNT8A excluding the nanodisc, resulting in a final 3.19 Å density map (See Fig. S2). Density modification was performed on unfiltered half maps using phenix.resolve_cryo_em (Terwilliger et al., 2020).

Structural model building and refinement—To build the WNT8A-WLS model we first made threaded a homology model of WNT8A based on the xWnt8 structure (PDB ID 4F0A) using CHAINSAW (Stein, 2008). The model was fitted to the map as a rigid body in Chimera (Pettersen et al., 2004) and transferred to Coot (Emsley et al., 2010; Emsley and Cowtan, 2004) for manual model building. A blurred map was used for some regions of WNT8A (i.e. residue 241–247, 288–310, 328–337) as this map was easier to interpret in these regions, and a blurred map (B=100) has been deposited to EMDB. We observed extra density that could not be accounted for by the protein extending out from two residues N103 and N262, and we were able to fit NAG and mannose moieties into this density consistent with predicted glycosylation sites (Emsley and Crispin, 2018). The palmitoleate (PAM) is attached to Ser186, as predicted, and the lipid chain was modeled into the density. WLS was modelled *de novo* in Coot using secondary structure predictions from the XtalPred server (Slabinski et al., 2007) as a guide. Subsequent model refinement and adjustment was performed in Coot and Phenix (Adams et al., 2010; Afonine et al., 2018) iteratively.

Model analysis—A cavity search using the Solvent Extractor from Voss Volume Voxelator server (Voss and Gerstein, 2010) was performed using an outer-probe radius of 15 Angstrom and inner-probe radius of 2 Angstrom. We used the DALI server to search for other structures with a similar fold both using only the transmembrane domain as well as

using the WLS-LD only (Holm, 2020). Chimera (Pettersen et al., 2004) and ChimeraX (Goddard et al., 2018) were used to visualize the structures in the figures.

Cell surface biotinylation—Membrane impermeable Sulfo-NHS-SS-Biotin (Thermo Scientific) was freshly dissolved in PBS/$Ca2^{+}$/$Mg2^{+}$ to 1 mg/ml before use. Transfected HEK293 cells were rinsed twice with PBS before adding the biotin solution on ice. The cells were incubated at 4 °C for 1 hour, followed by washing once with PBS/$Ca2^{+}$/$Mg2^{+}$. The reaction was quenched by incubating with 100 mM glycine at 4 °C for 15 minutes. After washing, the cells were lysed on the dish with HEPES lysis buffer (50 mM HEPES pH 7.4, 150 mM NaCl, 1 mM EDTA, 1 mM DTT, 0.6% NP-40 and protease inhibitor cocktail) for subsequent streptavidin pull down.

Immunoprecipitation—Transfected HEK293 cells were lysed with HEPES lysis buffer (50 mM HEPES pH 7.4, 150 mM NaCl, 1 mM EDTA, 1 mM DTT, 0.6% NP-40 and protease inhibitor cocktail) on ice. After removal of cell debris, 500 μg of total protein lysates were used for each immunoprecipitation with 1 μg of anti-V5 antibody (BioRad). After incubation in the cold room overnight with tumbling, 40 μl of Protein A/G plus agarose (Santa Cruz) was added into each tube and incubated for another 2 hours in the cold room. The agarose beads were then pelleted and washed three times with HEPES lysis buffer and bound proteins were eluted in SDS-PAGE sample buffer.

QUANTIFICATION AND STATISTICAL ANALYSIS

For calculations of Fourier shell correlations (FSC), the FSC cut-off criterion of 0.143 (Rosenthal and Henderson, 2003) was used. No statistical methods were used to predetermine sample size. The experiments were not randomized. The investigators were not blinded to allocation during experiments and outcome assessment. For cell-based assays, statistics were calculated using GraphPad Prism 8.

Supplementary Material

Refer to Web version on PubMed Central for supplementary material.

ACKNOWLEDGMENTS

We gratefully acknowledge the assistance of members of the Mancia and Virshup labs, and of the Columbia Cryo-EM facility. We thank Larry Shapiro, Frederic Bard and Nick Tolwinski, as well as Joseph Gleeson and Bruno Reversade and their respective groups for insightful comments and suggestions. This work was supported by NIH grants (R35 GM132120 to F.M.) and by the National Research Foundation Singapore, administered by the Singapore Ministry of Health's National Medical Research Council under Singapore Translational Research (STaR) Award MOH-000155 to D.M.V.

REFERENCES

Adams PD, Afonine PV, Bunkóczi G, Chen VB, Davis IW, Echols N, Headd JJ, Hung L-W, Kapral GJ, Grosse-Kunstleve RW, et al. (2010). PHENIX: a comprehensive Python-based system for macromolecular structure solution. Acta Crystallogr. D Biol. Crystallogr 66, 213–221. [PubMed: 20124702]

Afonine PV, Poon BK, Read RJ, Sobolev OV, Terwilliger TC, Urzhumtsev A, and Adams PD (2018). Real-space refinement in PHENIX for cryo-EM and crystallography. Acta Crystallogr Sect D Struct Biol 74, 531–544. [PubMed: 29872004]

Altschul SF, and Koonin EV (1998). Iterated profile searches with PSI-BLAST--a tool for discovery in protein databases. Trends Biochem. Sci 23, 444–447. [PubMed: 9852764]

Audet M, and Stevens RC (2019). Emerging structural biology of lipid G protein-coupled receptors. Protein Sci 28, 292–304. [PubMed: 30239054]

Bartscherer K, Pelte N, Ingelfinger D, and Boutros M (2006). Secretion of Wnt ligands requires Evi, a conserved transmembrane protein. Cell 125, 523–533. [PubMed: 16678096]

Bazan JF, Janda CY, and Garcia KC (2012). Structural architecture and functional evolution of wnts. Dev Cell 23, 227–232. [PubMed: 22898770]

Bänziger C, Soldini D, Schütt C, Zipperlen P, Hausmann G, and Basler K (2006). Wntless, a conserved membrane protein dedicated to the secretion of Wnt proteins from signaling cells. Cell 125, 509–522. [PubMed: 16678095]

Belenkaya TY, Wu Y, Tang X, Zhou B, Cheng L, Sharma YV, Yan D, Selva EM, and Lin X (2008). The retromer complex influences Wnt secretion by recycling wntless from endosomes to the trans-Golgi network. Dev Cell 14, 120–131. [PubMed: 18160348]

Carpenter AC, Rao S, Wells JM, Campbell K, and Lang RA (2010). Generation of mice with a conditional null allele for Wntless. Genesis 48, 554–558. [PubMed: 20614471]

Carugo O, Cemazar M, Zahariev S, Hudáky I, Gáspári Z, Perczel A, and Pongor S (2003). Vicinal disulfide turns. Protein Eng. 16, 637–639. [PubMed: 14560048]

Coombs GS, Schmitt AA, Canning CA, Utomo V, Toone EJ, and Virshup DM (2012). Modulation of Wnt/β-catenin signaling and proliferation by a ferrous iron chelator with therapeutic efficacy in genetically engineered mouse models of cancer. Oncogene 31, 213–225. [PubMed: 21666721]

Coombs GS, Yu J, Canning CA, Veltri CA, Covey TM, Cheong JK, Utomo V, Banerjee N, Zhang ZH, Jadulco RC, et al. (2010). WLS-dependent secretion of WNT3A requires Ser209 acylation and vacuolar acidification. J Cell Sci 123, 3357–3367. [PubMed: 20826466]

Deshpande I, Liang J, Hedeen D, Roberts KJ, Zhang Y, Ha B, Latorraca NR, Faust B, Dror RO, Beachy PA, et al. (2019). Smoothened stimulation by membrane sterols drives Hedgehog pathway activity. Nature 571, 284–288. [PubMed: 31263273]

Emsley P, and Crispin M (2018). Structural analysis of glycoproteins: building N-linked glycans with Coot. Acta Crystallogr Sect D Struct Biol 74, 256–263. [PubMed: 29652253]

Emsley P, Lohkamp B, Scott WG, and Cowtan K (2010). Features and development of Coot. Acta Crystallogr. D Biol. Crystallogr 66, 486–501. [PubMed: 20383002]

Emsley P, and Cowtan K (2004). Coot: model-building tools for molecular graphics. Acta Crystallogr. D Biol. Crystallogr 60, 2126–2132. [PubMed: 15572765]

Franch-Marro X, Wendler F, Guidato S, Griffith J, Baena-Lopez A, Itasaki N, Maurice MM, and Vincent J-P (2008). Wingless secretion requires endosome-to-Golgi retrieval of Wntless/Evi/Sprinter by the retromer complex. Nat. Cell Biol 10, 170–177. [PubMed: 18193037]

Fu J, Jiang M, Mirando AJ, Yu H-MI, and Hsu W (2009). Reciprocal regulation of Wnt and Gpr177/mouse Wntless is required for embryonic axis formation. Proc. Natl. Acad. Sci. U.S.a 106, 18598–18603. [PubMed: 19841259]

Gasnereau I, Herr P, Chia PZC, Basler K, and Gleeson PA (2011). Identification of an endocytosis motif in an intracellular loop of wntless protein, essential for its recycling and the control of wnt protein signaling. J Biol Chem 286, 43324–43333. [PubMed: 22027831]

Gloriam DE, Fredriksson R, and Schiöth HB (2007). The G protein-coupled receptor subset of the rat genome. BMC Genomics 8, 338. [PubMed: 17892602]

Goddard TD, Huang CC, Meng EC, Pettersen EF, Couch GS, Morris JH, and Ferrin TE (2018). UCSF ChimeraX: Meeting modern challenges in visualization and analysis. Protein Sci 27, 14–25. [PubMed: 28710774]

Goehring A, Lee C-H, Wang KH, Michel JC, Claxton DP, Baconguis I, Althoff T, Fischer S, Garcia KC, and Gouaux E (2014). Screening and large-scale expression of membrane proteins in mammalian cells for structural studies. Nat Protoc 9, 2574–2585. [PubMed: 25299155]

Goodman RM, Thombre S, Firtina Z, Gray D, Betts D, Roebuck J, Spana EP, and Selva EM (2006). Sprinter: a novel transmembrane protein required for Wg secretion and signaling. Development 133, 4901–4911. [PubMed: 17108000]

Gross JC, Chaudhary V, Bartscherer K, and Boutros M (2012). Active Wnt proteins are secreted on exosomes. Nat. Cell Biol 14, 1036–1045. [PubMed: 22983114]

Grzeschik K, Bornholdt D, Oeffner F, König A, del Carmen Boente M, Enders H, Fritz B, Hertl M, Grasshoff U, Höfling K, et al. (2007). Deficiency of PORCN, a regulator of Wnt signaling, is associated with focal dermal hypoplasia. Nat Genet 39, 833–835. [PubMed: 17546031]

Hannoush RN (2015). Synthetic protein lipidation. Current Opinion in Chemical Biology 28, 39–46. [PubMed: 26080277]

Herr P, and Basler K (2012). Porcupine-mediated lipidation is required for Wnt recognition by Wls. Dev Biol 361, 392–402. [PubMed: 22108505]

Hirai H, Matoba K, Mihara E, Arimori T, and Takagi J (2019). Crystal structure of a mammalian Wnt-frizzled complex. Nat Struct Mol Biol 26, 372–379. [PubMed: 31036956]

Holm L (2020). DALI and the persistence of protein shape. Protein Sci 29, 128–140. [PubMed: 31606894]

Hoppler S, Brown JD, and Moon RT (1996). Expression of a dominant-negative Wnt blocks induction of MyoD in Xenopus embryos. Genes Dev 10, 2805–2817. [PubMed: 8946920]

Huang P, Zheng S, Wierbowski BM, Kim Y, Nedelcu D, Aravena L, Liu J, Kruse AC, and Salic A (2018). Structural Basis of Smoothened Activation in Hedgehog Signaling. Cell 174, 312–324.e316. [PubMed: 29804838]

Hunter HN, Fulton DB, Ganz T, and Vogel HJ (2002). The solution structure of human hepcidin, a peptide hormone with antimicrobial activity that is involved in iron uptake and hereditary hemochromatosis. J Biol Chem 277, 37597–37603. [PubMed: 12138110]

Janda CY, Waghray D, Levin AM, Thomas C, and Garcia KC (2012). Structural Basis of Wnt Recognition by Frizzled. Science 337, 59–64. [PubMed: 22653731]

Kadowaki T, Wilder E, Klingensmith J, Zachary K, and Perrimon N (1996). The segment polarity gene porcupine encodes a putative multitransmembrane protein involved in Wingless processing. Genes Dev 10, 3116–3128. [PubMed: 8985181]

Kakugawa S, Langton PF, Zebisch M, Howell S, Chang T-H, Liu Y, Feizi T, Bineva G, O'Reilly N, Snijders AP, et al. (2015). Notum deacylates Wnt proteins to suppress signalling activity. Nature 519, 187–192. [PubMed: 25731175]

Koles K, Nunnari J, Li Y, and Leszyk J (2012). Mechanism of evenness interrupted (Evi)-exosome release at synaptic boutons. J Biol Chem 287, 16820–16834. [PubMed: 22437826]

Korkut C, Ataman B, Barria R, and Budnik V (2009). Trans-synaptic transmission of vesicular Wnt signals through Evi/Wntless. Cell 139, 393–404. [PubMed: 19837038]

Kumar S, Žigman M, Patel TR, Trageser B, Gross JC, Rahm K, Boutros M, Gradl D, Steinbeisser H, Holstein T, et al. (2014). Molecular dissection of Wnt3a-Frizzled8 interaction reveals essential and modulatory determinants of Wnt signaling activity. BMC Biol. 12, 44–17. [PubMed: 24885675]

Kusserow A, Pang K, Sturm C, Hrouda M, Lentfer J, Schmidt HA, Technau U, Haeseler, von A, Hobmayer B, Martindale MQ, et al. (2005). Unexpected complexity of the Wnt gene family in a sea anemone. Nature 433, 156–160. [PubMed: 15650739]

Lander GC, Stagg SM, Voss NR, Cheng A, Fellmann D, Pulokas J, Yoshioka C, Irving C, Mulder A, Lau P-W, et al. (2009). Appion: an integrated, database-driven pipeline to facilitate EM image processing. Journal of Structural Biology 166, 95–102. [PubMed: 19263523]

Langton PF, Kakugawa S, and Vincent J-P (2016). Making, Exporting, and Modulating Wnts. Trends Cell Biol 26, 756–765. [PubMed: 27325141]

Lee C-J, Rana MS, Bae C, Li Y, and Banerjee A (2019). In vitro reconstitution of Wnt acylation reveals structural determinants of substrate recognition by the acyltransferase human Porcupine. J Biol Chem 294, 231–245. [PubMed: 30420431]

Loh KM, van Amerongen R, and Nusse R (2016). Generating Cellular Diversity and Spatial Form: Wnt Signaling and the Evolution of Multicellular Animals. Dev Cell 38, 643–655. [PubMed: 27676437]

Luken BM, Winn LYN, Emsley J, Lane DA, and Crawley JTB (2010). The importance of vicinal cysteines, C1669 and C1670, for von Willebrand factor A2 domain function. Blood 115, 4910–4913. [PubMed: 20354169]

Macdonald BT, Hien A, Zhang X, Iranloye O, Virshup DM, Waterman ML, and He X (2014). Disulfide bond requirements for active Wnt ligands. J Biol Chem 289, 18122–18136. [PubMed: 24841207]

Madan B, Ke Z, Harmston N, Ho SY, Frois AO, Alam J, Jeyaraj DA, Pendharkar V, Ghosh K, Virshup IH, et al. (2016). Wnt addiction of genetically defined cancers reversed by PORCN inhibition. Oncogene 35, 2197–2207. [PubMed: 26257057]

McGough IJ, Vecchia L, Bishop B, Malinauskas T, Beckett K, Joshi D, O'Reilly N, Siebold C, Jones EY, and Vincent J-P (2020). Glypicans shield the Wnt lipid moiety to enable signalling at a distance. Nature 423, 448.

Moti N, Yu J, Boncompain G, Perez F, and Virshup DM (2019). Wnt traffic from endoplasmic reticulum to filopodia. PLoS ONE 14, e0212711. [PubMed: 30794657]

Najdi R, Proffitt K, Sprowl S, Kaur S, Yu J, Covey TM, Virshup DM, and Waterman ML (2012). A uniform human Wnt expression library reveals a shared secretory pathway and unique signaling activities. Differentiation 84, 203–213. [PubMed: 22784633]

Niehrs C (2012). The complex world of WNT receptor signalling. Nat Rev Mol Cell Biol 13, 767–779. [PubMed: 23151663]

Nile AH, Mukund S, Stanger K, Wang W, and Hannoush RN (2017). Unsaturated fatty acyl recognition by Frizzled receptors mediates dimerization upon Wnt ligand binding. Proc. Natl. Acad. Sci. U.S.a 114, 4147–4152. [PubMed: 28377511]

Panáková D, Sprong H, Marois E, Thiele C, and Eaton S (2005). Lipoprotein particles are required for Hedgehog and Wingless signalling. Nature 435, 58–65. [PubMed: 15875013]

Papasergi-Scott MM, Robertson MJ, Seven AB, Panova O, Mathiesen JM, and Skiniotis G (2020). Structures of metabotropic GABAB receptor. Nature 584, 310–314. [PubMed: 32580208]

Park J, Fu Z, Frangaj A, Liu J, Mosyak L, Shen T, Slavkovich VN, Ray KM, Taura J, Cao B, et al. (2020). Structure of human GABAB receptor in an inactive state. Nature 84, 835–836.

Pettersen EF, Goddard TD, Huang CC, Couch GS, Greenblatt DM, Meng EC, and Ferrin TE (2004). UCSF Chimera--a visualization system for exploratory research and analysis. J Comput Chem 25, 1605–1612. [PubMed: 15264254]

Punjani A, Rubinstein JL, Fleet DJ, and Brubaker MA (2017). cryoSPARC: algorithms for rapid unsupervised cryo-EM structure determination. Nat Meth 14, 290–296.

Reeves PJ, Callewaert N, Contreras R, and Khorana HG (2002). Structure and function in rhodopsin: high-level expression of rhodopsin with restricted and homogeneous N-glycosylation by a tetracycline-inducible N-acetylglucosaminyltransferase I-negative HEK293S stable mammalian cell line. Proc. Natl. Acad. Sci. U.S.A 99, 13419–13424. [PubMed: 12370423]

Rios-Esteves J, and Resh MD (2013). Stearoyl CoA Desaturase Is Required to Produce Active, Lipid-Modified Wnt Proteins. Cell Reports 4, 1072–1081. [PubMed: 24055053]

Rosenthal PB, and Henderson R (2003). Optimal determination of particle orientation, absolute hand, and contrast loss in single-particle electron cryomicroscopy. J Mol Biol 333, 721–745. [PubMed: 14568533]

Routledge D, and Scholpp S (2019). Mechanisms of intercellular Wnt transport. Development 146, 1–10.

Slabinski L, Jaroszewski L, Rychlewski L, Wilson IA, Lesley SA, and Godzik A (2007). XtalPred: a web server for prediction of protein crystallizability. Bioinformatics 23, 3403–3405. [PubMed: 17921170]

Smotrys JE, and Linder ME (2004). Palmitoylation of intracellular signaling proteins: regulation and function. Annu Rev Biochem 73, 559–587. [PubMed: 15189153]

Stanganello E, and Scholpp S (2016). Role of cytonemes in Wnt transport. J Cell Sci 129, 665–672. [PubMed: 26823607]

Stein N (2008). CHAINSAW: a program for mutating pdb files used as templates in molecular replacement. J Appl Crystallogr 41, 641–643.

Sui X, Arlt H, Brock KP, Lai ZW, DiMaio F, Marks DS, Liao M, Farese RV, and Walther TC (2018). Cryo-electron microscopy structure of the lipid droplet-formation protein seipin. J Cell Biol 217, 4080–4091. [PubMed: 30327422]

Sui X, Wang K, Gluchowski NL, Elliott SD, Liao M, Walther TC, and Farese RV (2020). Structure and catalytic mechanism of a human triacylglycerol-synthesis enzyme. Nature 332, 1–6.

Suloway C, Pulokas J, Fellmann D, Cheng A, Guerra F, Quispe J, Stagg S, Potter CS, and Carragher B (2005). Automated molecular microscopy: the new Leginon system. Journal of Structural Biology 151, 41–60. [PubMed: 15890530]

Swiatek W, Kang H, Garcia BA, Shabanowitz J, Coombs GS, Hunt DF, and Virshup DM (2006). Negative regulation of LRP6 function by casein kinase I epsilon phosphorylation. J Biol Chem 281, 12233–12241. [PubMed: 16513652]

Takada R, Satomi Y, Kurata T, Ueno N, Norioka S, Kondoh H, Takao T, and Takada S (2006). Monounsaturated fatty acid modification of Wnt protein: its role in Wnt secretion. Dev Cell 11, 791–801. [PubMed: 17141155]

Terwilliger TC, Ludtke SJ, Read RJ, Adams PD, and Afonine PV (2020). Improvement of cryo-EM maps by density modification. Nat Meth 17, 923–927.

Tuladhar R, Yarravarapu N, Ma Y, Zhang C, Herbert J, Kim J, Chen C, and Lum L (2019). Stereoselective fatty acylation is essential for the release of lipidated WNT proteins from the acyltransferase Porcupine (PORCN). J Biol Chem 294, 6273–6282. [PubMed: 30737280]

van den Heuvel M, Harryman-Samos C, Klingensmith J, Perrimon N, and Nusse R (1993). Mutations in the segment polarity genes wingless and porcupine impair secretion of the wingless protein. Embo J 12, 5293–5302. [PubMed: 8262072]

Veeman MT, Axelrod JD, and Moon RT (2003). A second canon. Functions and mechanisms of beta-catenin-independent Wnt signaling. Dev Cell 5, 367–377. [PubMed: 12967557]

Voss NR, and Gerstein M (2010). 3V: cavity, channel and cleft volume calculator and extractor. Nucleic Acids Res 38, W555–W562. [PubMed: 20478824]

Wang H, Klein MG, Zou H, Lane W, Snell G, Levin I, Li K, and Sang B-C (2015). Crystal structure of human stearoyl-coenzyme A desaturase in complex with substrate. Nat Struct Mol Biol 22, 581–585. [PubMed: 26098317]

Wang X, Reid Sutton V, Omar Peraza-Llanes J, Yu Z, Rosetta R, Kou Y, Eble T, Patel A, Thaller C, Fang P, et al. (2007). Mutations in X-linked PORCN, a putative regulator of Wnt signaling, cause focal dermal hypoplasia. Nat Genet 39, 836–838. [PubMed: 17546030]

Waterhouse AM, Procter JB, Martin DMA, Clamp M, and Barton GJ (2009). Jalview Version 2--a multiple sequence alignment editor and analysis workbench. Bioinformatics 25, 1189–1191. [PubMed: 19151095]

Willert K, Brown JD, Danenberg E, Duncan AW, Weissman IL, Reya T, Yates JR, and Nusse R (2003). Wnt proteins are lipid-modified and can act as stem cell growth factors. Nature 423, 448–452. [PubMed: 12717451]

Xu Q, Wang Y, Dabdoub A, Smallwood PM, Williams J, Woods C, Kelley MW, Jiang L, Tasman W, Zhang K, et al. (2004). Vascular development in the retina and inner ear: control by Norrin and Frizzled-4, a high-affinity ligand-receptor pair. Cell 116, 883–895. [PubMed: 15035989]

Yamamoto H, Hanaki H, Sakane H, and Tsujimoto I (2013). The apical and basolateral secretion of Wnt11 and Wnt3a in polarized epithelial cells is regulated by different mechanisms. J Cell Sci 126, 2931–2943. [PubMed: 23613470]

Yan R, Qian H, Lukmantara I, Gao M, Du X, Yan N, and Yang H (2018). Human SEIPIN Binds Anionic Phospholipids. Dev Cell 47, 248–256.e4. [PubMed: 30293840]

Yang S, Wu Y, Xu T-H, de Waal PW, He Y, Pu M, Chen Y, DeBruine ZJ, Zhang B, Zaidi SA, et al. (2018). Crystal structure of the Frizzled 4 receptor in a ligand-free state. Nature 560, 666–670. [PubMed: 30135577]

Yu J, Chia J, Canning CA, Jones CM, Bard FA, and Virshup DM (2014). WLS retrograde transport to the endoplasmic reticulum during Wnt secretion. Dev Cell 29, 277–291. [PubMed: 24768165]

Zhang H, Qiao A, Yang L, Van Eps N, Frederiksen KS, Yang D, Dai A, Cai X, Zhang H, Yi C, et al. (2018a). Structure of the glucagon receptor in complex with a glucagon analogue. Nature 553, 106–110. [PubMed: 29300013]

Zhang X, Dong S, and Xu F (2018b). Structural and Druggability Landscape of Frizzled G Protein-Coupled Receptors. Trends Biochem. Sci 43, 1033–1046. [PubMed: 30309741]

Zhong Z, Zylstra-Diegel CR, Schumacher CA, Baker JJ, Carpenter AC, Rao S, Yao W, Guan M, Helms JA, Lane NE, et al. (2012). Wntless functions in mature osteoblasts to regulate bone mass. Proc. Natl. Acad. Sci. U.S.a 109, E2197–E2204. [PubMed: 22745162]

Zhong Z, and Virshup DM (2020). Wnt Signaling and Drug Resistance in Cancer. Mol Pharmacol 97, 72–89. [PubMed: 31787618]

Highlights

- We present the cryo-EM structure of human WNT8A in complex with its transporter WLS
- The WLS membrane domain has structural homology to GPCRs
- WLS harbors the Wnt palmitoleate in a hydrophobic cavity within its membrane domain
- A conformational switch on Wnt hairpin 3 may favor unidirectional Wnt transfer

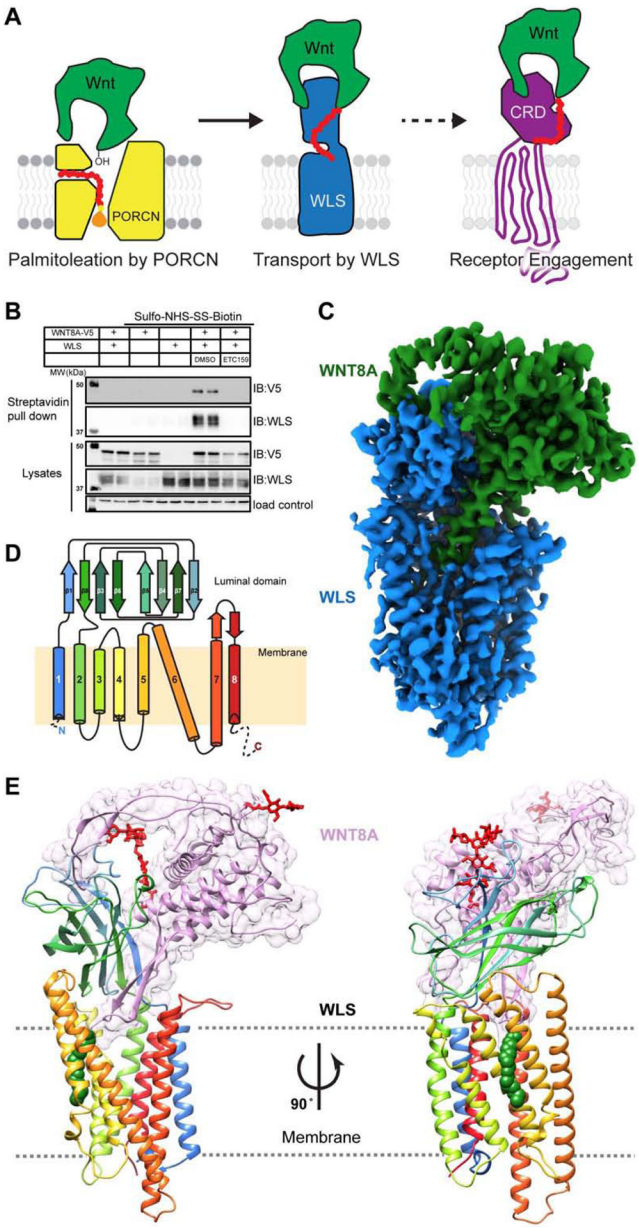

Figure 1. Single particle cryo-EM structure of WNT8A in complex with WLS.

(A) The journey of Wnt. The palmitoleoyl moiety (red chain) is transferred by PORCN from CoA (orange ball) to Wnt in the ER. Acylated Wnt then binds to WLS, which transports the complex to the plasma membrane, where Wnt, perhaps in a multistep process, is transferred to receptors, illustrated here as CRD-containing FZD, on the signal-receiving cells.

(B) The WNT8A-WLS complex carries palmitoleated Wnt to the plasma membrane. Western blot analysis showing cell surface biotinylation of HEK293 cells ectopically expressing V5-tagged WNT8A and WLS as indicated. 100 nM PORCN inhibitor ETC-159 was added 6 hours after plasmid transfection.

(**C**) Cryo-EM density map of the WNT8A-WLS complex. The cryo-EM density corresponding to WLS is in blue, and to WNT8A is in green.

(**D)** Topology of WLS highlighting the eight TM helices and the luminal domain (LD) loop comprised of 8 β-sheets arranged in a β–sandwich. Disordered regions are shown as dotted lines and coloring is in rainbow from N- (blue) to C- (red) terminus.
(**E)** The 3.2 Å structure of WNT8A bound to WLS with WLS colored in rainbow as in **D**, and WNT8A in violet with a transparent surface. The PAM is represented as green spheres extending out between TM helices 4 and 5. Glycosylation of WNT8A at two sites is in red, represented as sticks.

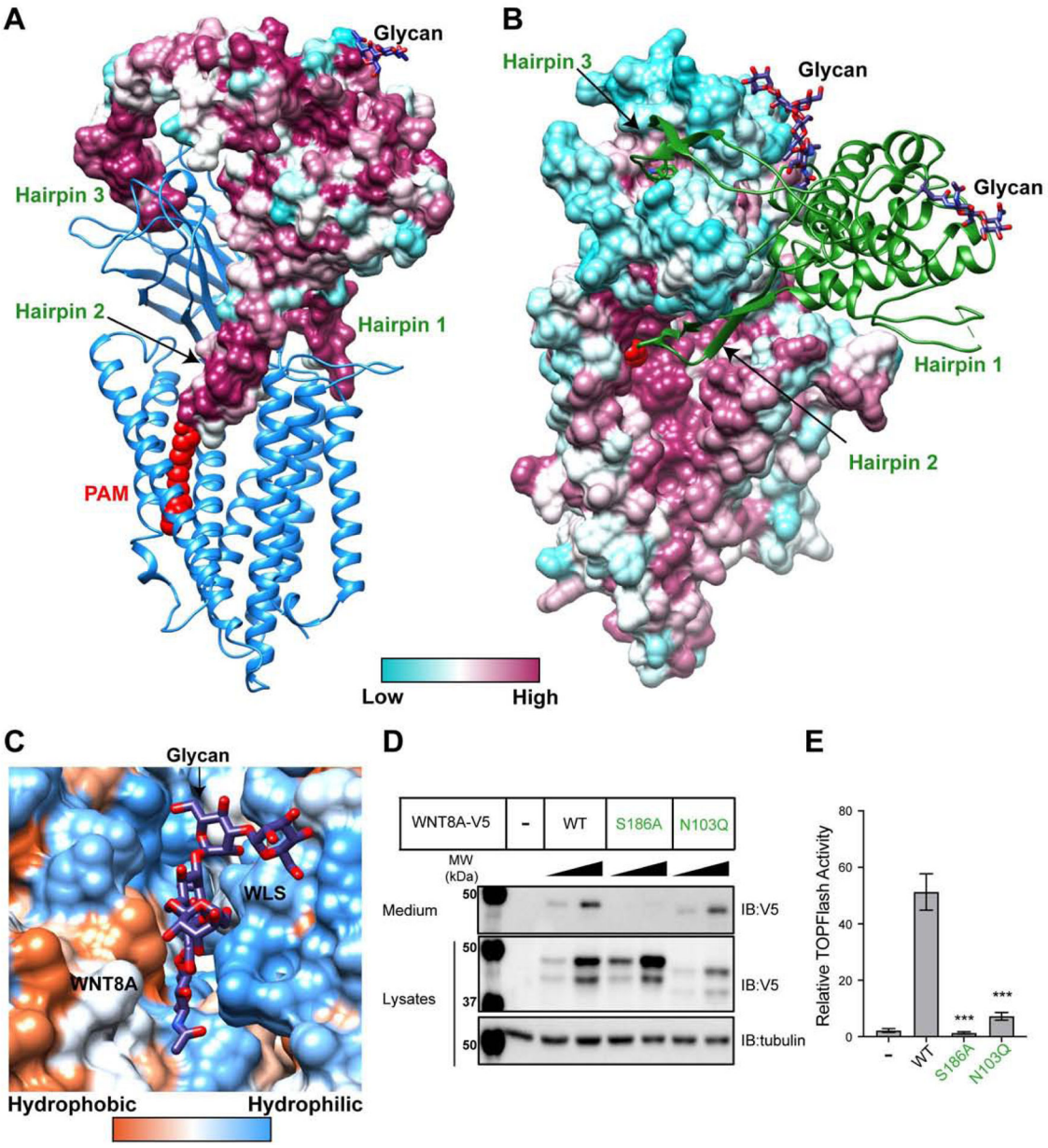

Figure 2. Glycosylated WNT8A interacts with WLS via three highly conserved hairpin loops.

(**A**) WLS is represented as a blue ribbon and WNT8A as a spacefill surface colored by conservation, highlighting the invariant nature of the three hairpin loops interacting with WLS. Hairpins 1 and 2 are separated by the WLS-LD. The PAM is depicted as red spheres.

(**B**) WNT8A in ribbon representation in green and WLS as a space fill surface colored by conservation, highlighting the conserved nature of the cavity between TM helices 4–7, the site for insertion of WNT8A hairpin 2.

(C) The glycan attached to Asn103 in WNT8A is sandwiched between a partially hydrophobic surface on WNT8A and a hydrophilic one on WLS-LD.

(**D**) Loss of the glycan at Asn103 did not affect WNT8A secretion. The indicated WNT8A-V5 constructs were transiently expressed in HEK293 cells which stably expressing the Wnt

reporter SuperTopFlash (STF). Conditioned medium was collected 48 hours post-transfection to assess WNT8A secretion. Acylation-defective mutant S186A was included as a negative control for secretion and signaling.

(**E**) The glycosylation-deficient WNT8A (N103Q) has reduced ability to signal. The indicated WNT8A proteins were transiently expressed in STF cells in the presence of RSPO3, which increases STF sensitivity to Wnt signals. The experiment was performed in triplicate and error bars indicate standard deviation. Unpaired t-test was used for statistical analysis. ***, p-value <0.001.

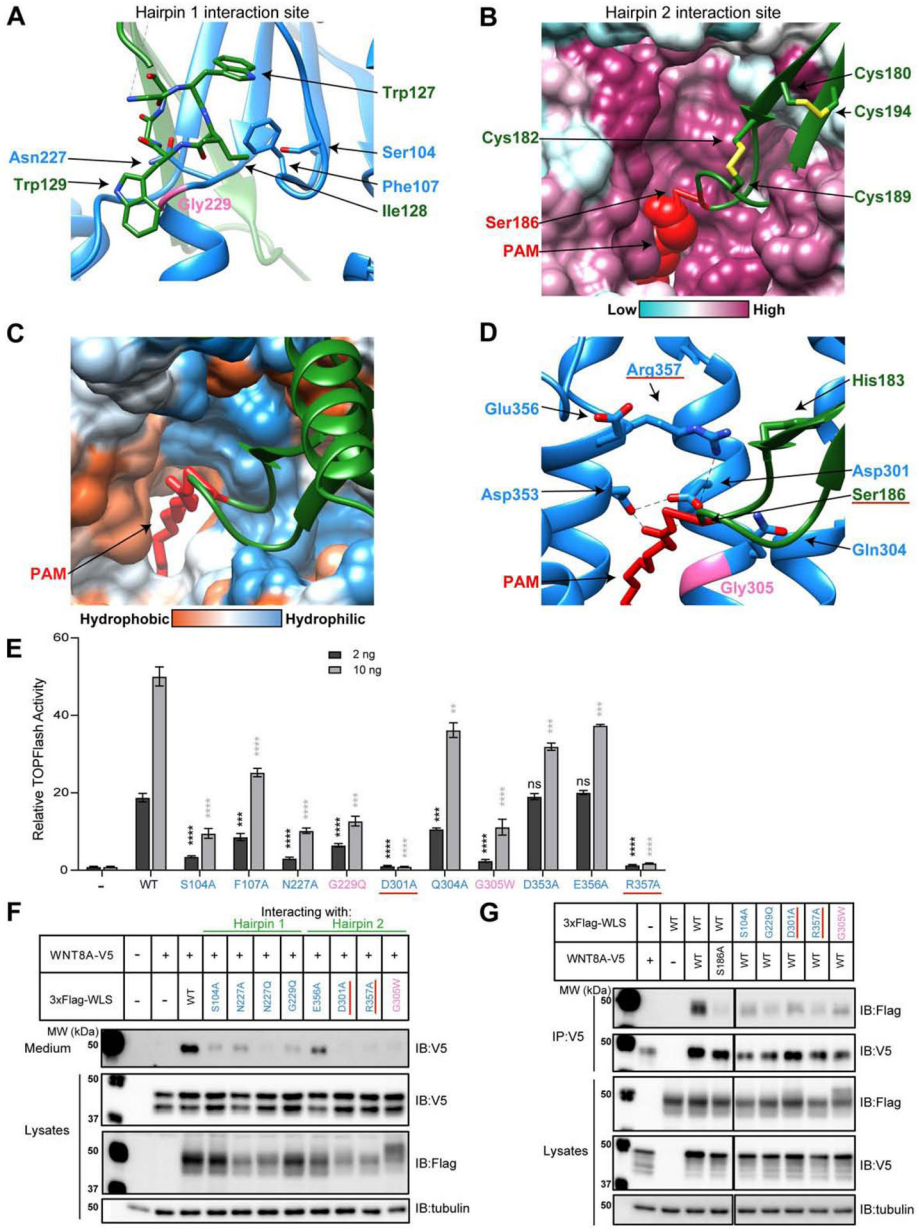

Figure 3. The interface between WLS and WNT8A

(A) Close-up view of WLS and WNT8A hairpin 1 interaction site. WLS is shown as a blue ribbon and WNT8A hairpins are shown as green ribbons. The conserved residues at the interface are shown as sticks.

(B) Close-up view of the WLS binding pocket for WNT8A hairpin 2, with WLS in spacefill representation colored by conservation, and WNT8A shown as green ribbon with the residues of hairpin 2 and its conserved disulfide bonds shown as sticks. The PAM is in red spacefill

(C) The WLS TM domain binding pocket is rendered as a surface, colored by hydrophobicity. Hairpin 2 of WNT8A is represented as a ribbon in green and the PAM as sticks in red.

(**D**) Close-up view of WLS and WNT8A hairpin 2 interaction site. WLS is shown as a blue ribbon and WNT8A hairpin 2 shown as a green ribbon. The conserved residues at the interface are shown as sticks and the PAM as red sticks.

(**E**) Mutation of contact points on WLS impacts Wnt/β-catenin signaling. The indicated WLS proteins with an internal 3x Flag-tag were expressed in RKO *WLS* null cells together with WNT3A and a TOPFlash reporter. Luciferase activities were measured 48 hours post-transfection. Mutants D301A and R357A (underlined in red) showed the most reduced activities. The experiment was performed in triplicate and error bars indicate standard deviation. Unpaired t-test was used for statistical analysis for each mutant comparing with WT WLS. ***, p-value <0.001; ****, p-value <0.0001; ns, non-significant.

(F) WLS residues at the interface with Wnt hairpins 1 and 2 are important for Wnt secretion. The indicated 3x-Flag-tagged WLS proteins were expressed in RKO *WLS* null cells together with WNT8A-V5, and conditioned media was collected 48 hours post-transfection to assess WNT8A secretion as in Figure 2. Mutating residues of WLS that interact with WNT8A hairpin 1 or 2 abolishes its secretion.

(**G**) WLS residues at the interface with Wnt hairpins 1 and 2 are important for binding to WNT8A. The indicated proteins were co-expressed in HEK293 cells, with the WNT8A acylation-defective mutant S186A as a negative control. Cells were lysed 48 hours post-transfection and anti-V5 antibody was used for immunoprecipitation. All lanes are from the same gels, with intervening lanes spliced out for clarity of presentation.

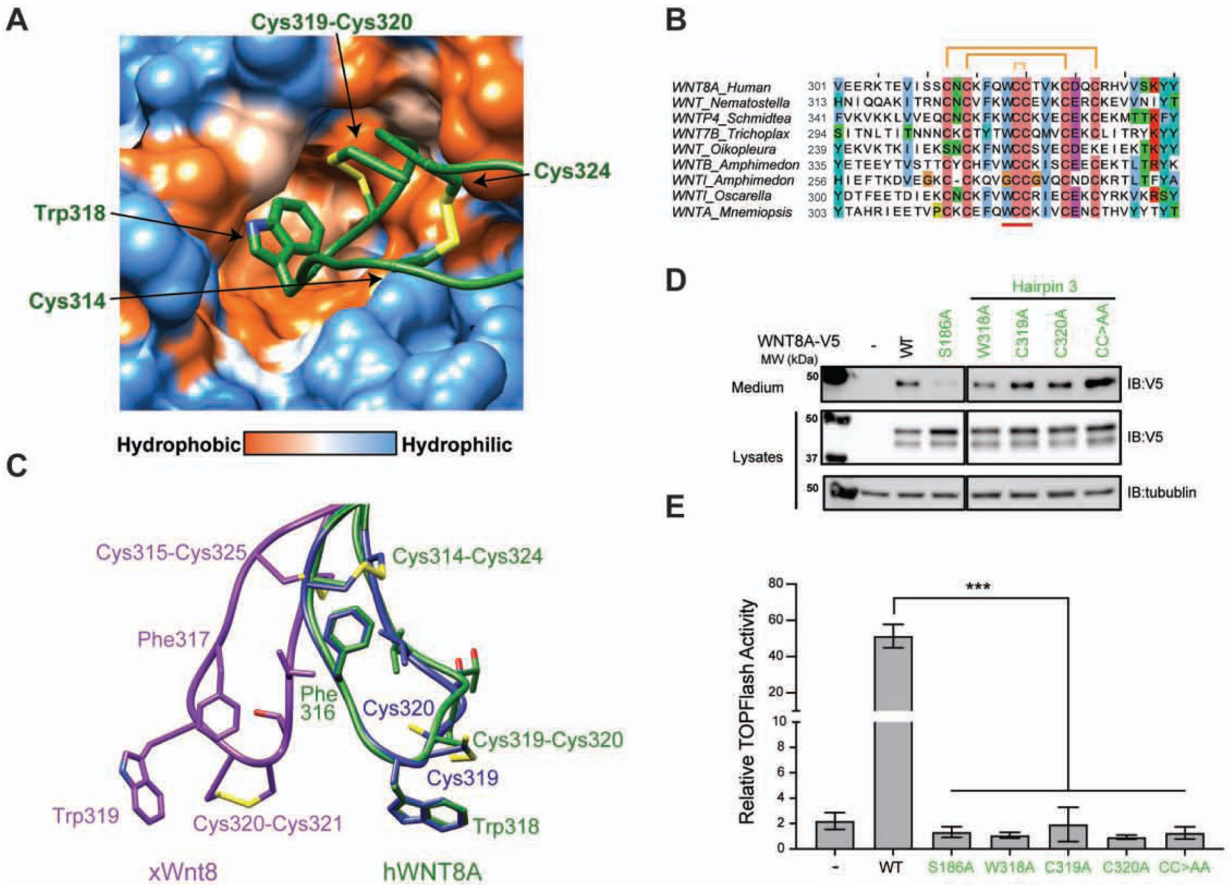

Figure 4. A conformational switch in Wnt Hairpin 3

(**A)** WNT8A hairpin 3, shown as green ribbon and amino acids as sticks, inserts into a hydrophobic pocket of WLS-LD, in surface representation colored by hydrophobicity.

(B) Broad conservation of the WCC motif (underlined) in Wnt hairpin 3. Selected sequences from diverse phyla including Trichoplax and sponges are aligned. Orange lines indicate disulfide bond formation. Adapted from (Bazan et al., 2012).

(C) The conserved aromatic residues at the tip of Wnt hairpin 3 change conformation moving from WLS to FZD. hWNT8A (from the WNT8A-WLS structure) and xWnt8 (from the Wnt8-FZD structure) are compared. These conformational changes occur irrespective of the oxidation status of the vicinal cysteines in hWNT8A. hWNT8A is shown with cysteines modelled as forming disulfides or reduced, as ribbon and sticks in blue and green, respectively. xWnt8 is shown as purple ribbon and sticks.

(D) WNT8A hairpin 3 is not required for secretion. WT or indicated WNT8A mutants were transfected into H. Medium was collected 48 hours post-transfection to assess WNT8A secretion. CC>AA, C319A C320A double mutant.

(E) Mutation of the WNT8A hairpin 3 abolishes β-catenin signaling activity. WT or indicated WNT8A-V5 mutants were expressed in STF cells together with RSPO3, and TOPFlash activity was assessed. The controls (no Wnt, WT and S186A) are as shown in Figure 2E as this was part of the same experiment. The experiment was performed in

triplicates and error bars indicate standard deviation. Unpaired t-test was used for statistical analysis for each mutant comparing with WT WNT8A. ***, p-value <0.001.

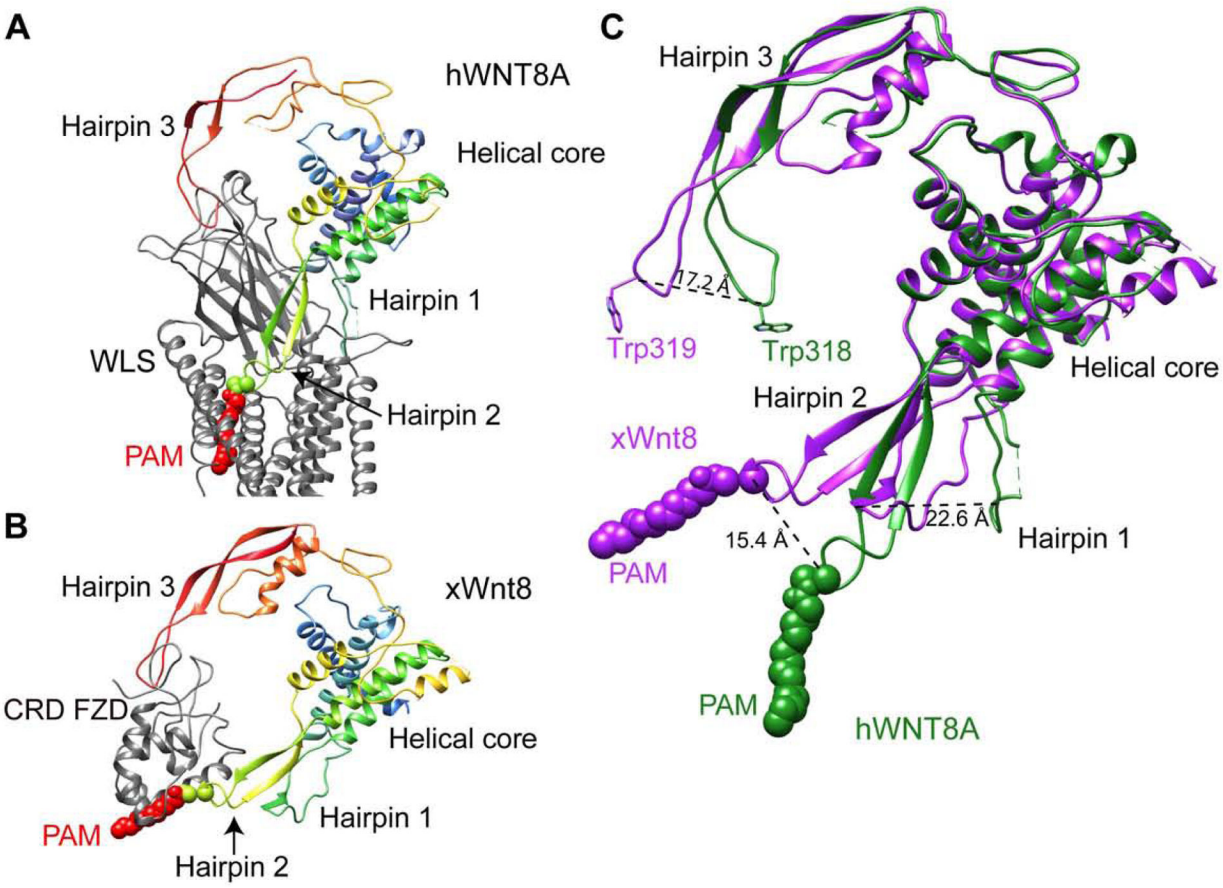

Figure 5. Wnt hairpins shift in the move from WLS to the FZD CRD.

(A) hWNT8A-WLS complex rendered in ribbon with hWNT8A colored in rainbow color and WLS in grey. PAM in depicted as red spheres.

(B) xWnt8-FZD CRD complex shown in ribbon with xWnt8 in rainbow and FZD CRD in grey (PDB ID 4F0A). PAM shown as in panel A.

(C) hWNT8A (in green) and xWnt8 (in purple) structures superimposed. Hairpin 1 and 2 are split apart in the hWNT8A structure compared to the xWnt8 structure, and hairpin 3 is tilted towards the helical core in hWNT8A compared to xWnt8.

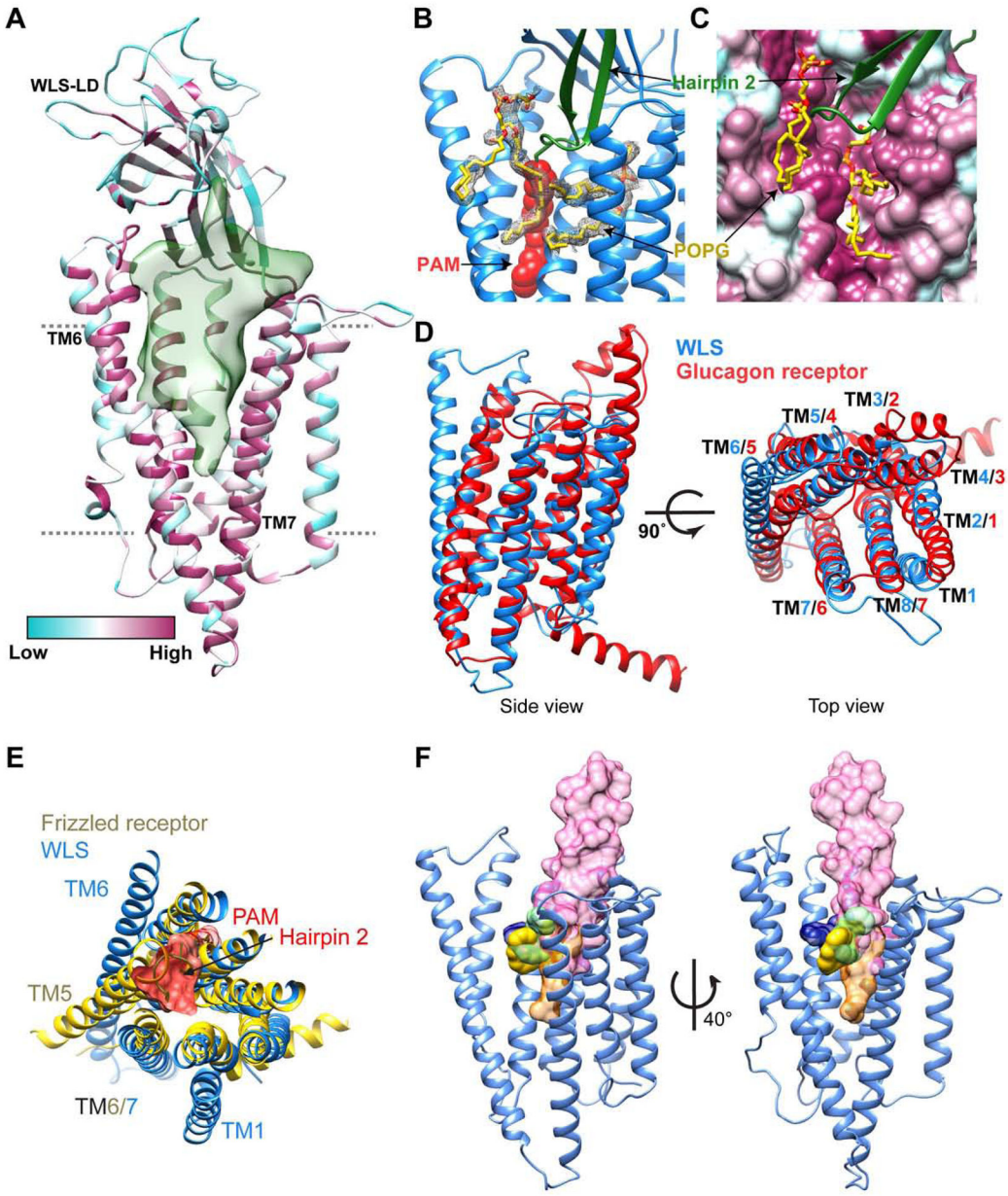

Figure 6. The WLS TM domain has homology to GPCRs with a conserved ligand-binding central cavity.

(A) Cavity in the TM domain of WLS shown as a semi-transparent green surface revealing a large opening (window) between TM6 and TM7 that directly exposes it to the lipid bilayer.

(**B)** Cavity region of WLS shown in blue ribbon with the PAM in red spheres and WNT8A hairpin 2 as green ribbon, revealing two ordered diacyl lipids (interpreted as POPG) represented as yellow sticks. The densities from the cryo-EM map corresponding to the POPG molecules are shown in mesh.

(**C)** Surface representation of WLS colored by conservation and the POPG lipids shown as yellow sticks.

(**D)** TM helices of WLS (blue) aligned with the TM helices of the glucagon receptor (red, PDB ID 5YQZ) shown both as sideview and as top view, rotated by 90 degrees.

(E) TM helices of WLS (blue) aligned with the TM region of the FZD4 (yellow) structure (PDB ID 6BD4) shown as ribbon. Hairpin 2 of WNT8A with PAM bound rendered as surface shown in red.

(F) To illustrate the potential drug-binding cavity of WLS, GPCRs with high structural homology to WLS that contained bound ligands were aligned with the WLS TM domain and the ligands were rendered in surface representation. The transmembrane domain of WLS is shown in blue ribbon. The ligand for β-2 adrenergic receptor is carazolol (yellow, from PDB ID 2RH1), for Glucagon receptor is NNC1702 (pink, from PDB 5YQZ), for Smoothened is SAG21k (orange, from PDB 6O3C), for cannabinoid receptor 2 is WIN55,212–2 (dark blue, from PDB 6PT0) and for δ-opioid receptor is naltrindole (green, from PDB 4N6H).

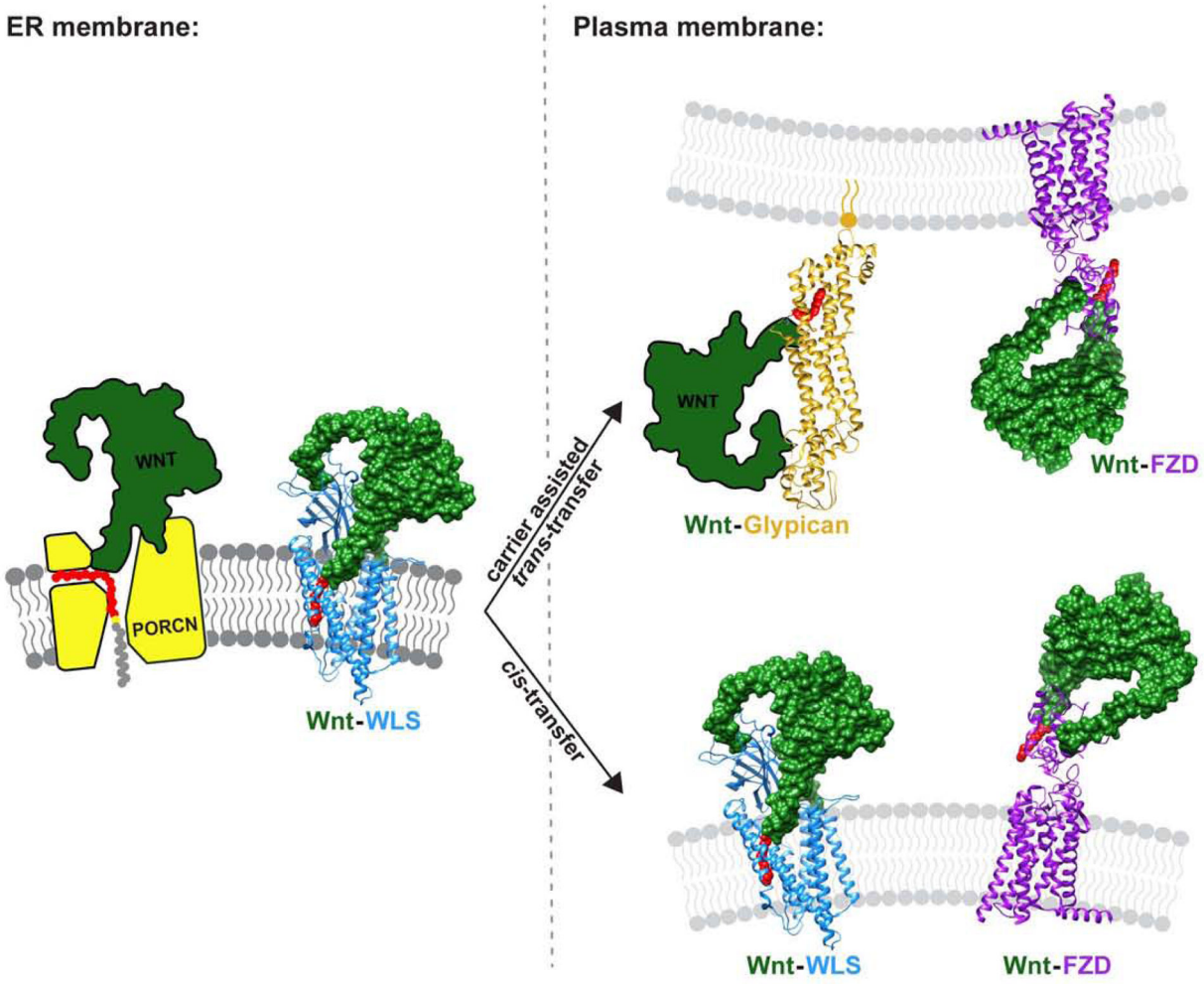

Figure 7. Implications for Wnt transfer

Following palmitoleation by PORCN, Wnt is transferred to WLS in the endoplasmic reticulum. The Wnt-WLS complex then traffics to the cell membrane, where several models of transfer of Wnt to FZD and coreceptors are possible. During autocrine signaling, Wnt may be transferred directly to an adjacent FZD in the plane of the membrane. In the *trans* model, Wnt disengages from WLS on the sending cells, and moves to the receiving cell, facilitated by carrier molecules such as glypicans and/or vesicles. In the *cis* model, the Wnt-WLS complex translocates to the receiving cell via vesicle traffic and membrane fusion, after which Wnt can transfer laterally from WLS to an adjacent FZD CRD. Alternative models are also possible. WLS is shown as a blue ribbon and Wnt as a green surface, with the PAM in red. FZD TM domain (PDB ID 6BD4) and FZD CRD domain (PDB ID 4F0A) are shown as purple ribbons.